Simultaneous Determination of Complex Permittivity and Permeability of Columnar Materials With Arbitrarily Shaped Cross Section

Hayato Miyagawa, Kikuo Wakino, *Life Fellow, IEEE*, Yu-De Lin, *Member, IEEE*, and Toshihide Kitazawa, *Senior Member, IEEE*

***Abstract*—An effective simultaneous evaluation method for the complex permittivity and permeability of lossy materials is proposed by applying it to an arbitrarily shaped cross-sectional post placed in a rectangular waveguide. We use one sample and only measure S_{21} parameters for two different locations of the sample. The measurement of complex reflection parameter S_{11} is not required in this evaluation method. The scheme of electromagnetic field analysis for the evaluation is based on the extended spectral-domain approach combined with the mode-matching method, which is accurate and efficient, and can be flexibly used for the iterative fitting operation for the estimation of material parameters. Sample preparation and setting is significantly easier in this method compared to conventional methods. The error caused by deviations in the setting of a sample is investigated. The estimated values for the sample material by this procedure show good agreement with the results obtained using the conventional method over the X-band.**

***Index Terms*—Arbitrarily shaped sample, hybrid method, inverse problem, permittivity and permeability, spectral-domain approach.**

I. Introduction

AN ACCURATE evaluation of the complex permittivity and permeability of materials is important for the design of broadband microwave devices and equipment. Over the past few decades, several evaluation methods have been reported for the electromagnetic (EM) properties of lossy materials using waveguides or coaxial lines [1]–[12]. For the simultaneous evaluation of $\dot{\varepsilon}_r$ and $\dot{\mu}_r$, conventional methods require data on both the S-parameters S_{11} and S_{21} of a sample [1]–[3], [5], [6], or the values of S_{11} or S_{21} for two samples with different lengths. The evaluation method with one sample is preferable to avoid errors due to material inhomogeneity [7], but it has required the complex S_{11}, as well as S_{21}, to evaluate complex $\dot{\varepsilon}_r$ and $\dot{\mu}_r$. The measurement of complex reflection parameter S_{11} requires precise knowledge of the position of the sample in a longitudinal direction with respect to the reference plane. Furthermore, measurement methods based on a simple transmission-line theory require the sample to be machined precisely to fill up the cross section of a guiding structure exactly. The air gap between the conductor and sample or the deformation due to the loading of an oversized soft sample gives rise to measurement errors [4]–[6], [8]. When the sample is a lossy and/or high permittivity or permeability material, the measured amplitude of S_{21} becomes very weak and degrades the accuracy of measurement data.

An alternative technique has been proposed to eliminate these problems by using the sample filling only a part of the waveguide cross section. This technique has been used to determine the complex permittivity [1], [3], [9] and both the complex permittivity and permeability [2], [10], [11]. Compared to the rectangular samples used in [10] and [11], the circular cylindrical sample used in [2] may be machined more easily, but it requires measurements of both complex S_{11} and S_{21}. The method in [12] is applicable to a sample with an arbitrarily shaped cross section placed at an arbitrary location in the waveguide cross section. However, it is restricted to the measurement of the complex permittivity.

In this paper, we extend the methods reported in [10] and [12] to evaluate the complex permittivity $\dot{\varepsilon}_r$ and permeability $\dot{\mu}_r$ of a columnar sample with an arbitrarily shaped cross section placed in a rectangular waveguide. We use one sample and measure S_{21} parameters for two different locations, e.g., with the sample placed in the center and near the sidewall of a waveguide. The complex reflection parameter S_{11}, which is more difficult to measure, is not required in this evaluation method. The measurement procedure is rather simple; however, the EM field analysis should be free from errors due to approximations in the calculation process and it should enhance the efficiency for the iterative fitting process of parameters with the measured data. The EM analysis used in this evaluation is a hybrid EM method proposed by the authors, combining the extended spectral-domain approach [13], [14] with the mode-matching method [15]. A hybrid method, which combines an open-space spectral method with the mode-matching method, was used for the analysis of obstacles in a rectangular waveguide [16]. EM fields are transformed by using the biorthogonal relation of eigenfunctions in Cartesian coordinates in the present method, while fields are expanded in terms of cylindrical functions in [2] and [16].

Manuscript received June 02, 2009; revised June 12, 2009. First published August 18, 2009; current version published September 04, 2009. This work was supported in part by the Kinki Mobile Radio Center Foundation under KMRC Research and Development Grant for Mobile Wireless.

H. Miyagawa, K. Wakino, and T. Kitazawa are with the Department of Electrical and Electronic Engineering, Ritsumeikan University, Kusatsu, Shiga 525-8577, Japan (e-mail: re012007@ed.ritsumei.ac.jp; k-wakino@poppy.ocn.ne.jp; kitazawa@se.ritsumei.ac.jp).

Y.-D. Lin is with the Department of Communication Engineering, National Chiao Tung University, Hsinchu 300, Taiwan (e-mail: ydlin@mail.nctu.edu.tw).

Color versions of one or more of the figures in this paper are available online at http://ieeexplore.ieee.org.

Digital Object Identifier 10.1109/TMTT.2009.2027201

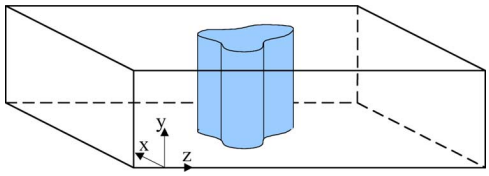

Fig. 1. Columnar sample with arbitrarily shaped cross section placed in waveguide.

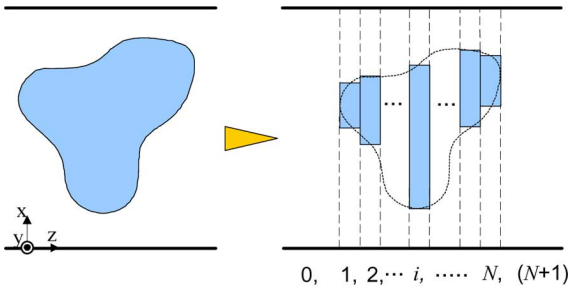

Fig. 2. Stairstep approximation of arbitrarily shaped cross section.

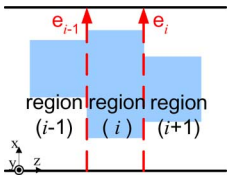

Fig. 3. Aperture electric fields.

II. EM Field Analysis

Fig. 1 shows a columnar sample with an arbitrarily shaped cross section placed in a rectangular waveguide. The sample may be a lossless or lossy dielectric and/or magnetic material. The dominant TE_{10} wave is incident upon the sample, and the scattered fields turned to be TE_{n0} modes are generated with a sample. The scattered fields are analyzed by the hybrid EM method, i.e., the extended spectral-domain approach combined with the mode-matching method [15].

In the present method, the sample holding region is divided into N thin slab regions (i) $(i = 1, \ldots, N$, as shown in Fig. 2). Each layer will be modeled as a thin rectangular waveguide loaded partially with a sample material. The aperture electric fields are introduced at each interface between the waveguide regions, as shown in Fig. 3, to fulfill the continuities of electric fields across the interfaces. Applying the equivalence theorem [17], each region can be treated independently. When the region is homogeneous and bounded by a perfect electric or magnetic wall [see Fig. 4(a)], the EM fields in the regions (regions 0 and $N + 1$ in Fig. 2) are expanded in terms of the simple eigenfunctions, i.e., sinusoidal functions, which satisfy the boundary conditions at the walls [see Fig. 4(a)]. However, in the ith region ($1 \leq i \leq N$ in Fig. 2), which contains a sample inhomogeneously, the fields cannot be expressed in terms of a set of simple sinusoidal functions. The eigenfunctions to express the fields in the inhomogeneous ith region can be constructed by using a mode-matching procedure. The eigenvalue equations are derived from the continuity conditions at the interfaces between

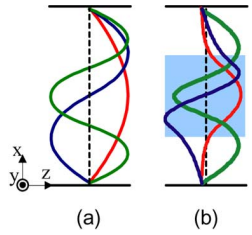

Fig. 4. First few eigenfunctions in the: (a) air region and (b) sample-loaded region.

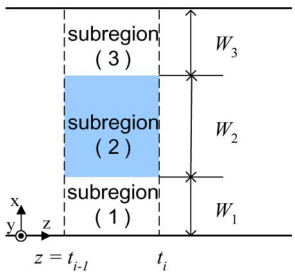

Fig. 5. Subregions in region (i).

the air and sample. Solving the eigenvalue equations numerically, the eigenfunctions, designated as $\Phi_m(x)$, are obtained and expressed in terms of the eigenvalues $\alpha_m^{(i1)}$, $\alpha_m^{(i2)}$, and $\alpha_m^{(i3)}$ in subregions (1)–(3) of the ith region (Fig. 5) as

$$\begin{aligned}
&\Phi_m(x) \\
&\quad = c_{1m}\frac{\sin\left(\alpha_m^{(i1)}x\right)}{\cos\left(\alpha_m^{(i1)}W_1\right)}, \qquad 0 \leq x \leq W_1 \\
&\Phi_m(x) \\
&\quad = \frac{c_{21m}\cos\left(\alpha_m^{(i2)}(x-a)\right) + c_{22m}\sin\left(\alpha_m^{(i2)}(x-a)\right)}{\cos\left(\alpha_m^{(i2)}(W_2-a)\right)}, \\
&\qquad W_1 \leq x \leq W_1 + W_2 \\
&\Phi_m(x) \\
&\quad = c_{3m}\frac{\sin(\alpha_m^{(i3)}(x-a))}{\cos(\alpha_m^{(i3)}(W_2+W_3-a))}, \qquad W_1+W_2 \leq x \leq a
\end{aligned} \tag{1}$$

where W_1, W_2, and W_3 are the widths of the subregions (Fig. 5), and c_{1m}, c_{21m}, c_{22m}, and c_{3m} are the normalization constants. The first few eigenfunctions are shown schematically in Fig. 4(b). When the subregions are composed of a substantially different material, for example, air and a material with loss and/or high permittivity, the eigenfunctions are localized inhomogeneously. These eigenfunctions do not satisfy a simple orthogonal relation. Instead, they satisfy the following biorthogonal relation in the entire ith region:

$$\begin{aligned}
\int_{W_1}\frac{\Phi_m(x)\Phi_n(x)}{\mu_{r1}}dx + \int_{W_2}\frac{\Phi_m(x)\Phi_n(x)}{\mu_{r2}}dx \\
+ \int_{W_3}\frac{\Phi_m(x)\Phi_n(x)}{\mu_{r3}}dx = \delta_{mn}
\end{aligned} \tag{2}$$

where μ_{r1}, μ_{r2}, and μ_{r3} are the permeabilities of the subregions and δ_{mn} is Kronecker's delta. The EM fields in the inhomogeneous ith region $(t_{i-1} \le z \le t_i)$ are expanded in terms of these eigenfunctions as

$$E_y^{(i)}(x,z) = \sum_{m=1}^{\infty} \Phi_m(x)\, \widetilde{E}_m^{(i)}(z)$$
$$H_x^{(i)}(x,z) = \sum_{m=1}^{\infty} \Phi_m(x)\, \widetilde{H}_m^{(i)}(z). \tag{3}$$

By utilizing the biorthogonal relation (2), the EM fields can be transformed into the spectral domain in a similar manner as in the homogeneous air region. In the transformed domain, EM fields can be easily related to the aperture fields

$$\widetilde{E}_m^{(i)}(z) = \widetilde{e}_{i-1} \frac{\sinh(\gamma_m(t_i - z))}{\sinh(\gamma_m(t_i - t_{i-1}))} + \widetilde{e}_i \frac{\sinh(\gamma_m(z - t_{i-1}))}{\sinh(\gamma_m(t_i - t_{i-1}))}$$
$$\widetilde{H}_m^{(i)}(z) = \frac{-\gamma_m}{j\omega\mu_0} \left\{ \widetilde{e}_{i-1} \frac{\cosh(\gamma_m(t_i - z))}{\sinh(\gamma_m(t_i - t_{i-1}))} - \widetilde{e}_i \frac{\cosh(\gamma_m(z - t_{i-1}))}{\sinh(\gamma_m(t_i - t_{i-1}))} \right\}$$
$$\gamma_m = \sqrt{\alpha_m^{(ik)2} - \omega^2 \varepsilon_0 \mu_0 \varepsilon_{rk} \mu_{rk}}, \qquad k = 1,2,3 \tag{4}$$

where $\widetilde{e}_i$ and $\widetilde{e}_{i-1}$ are the transformed aperture fields at $z = t_i$ and $z = t_{i-1}$ (Fig. 3), respectively,

$$\widetilde{e}_i = \int_0^a e_i(x) \frac{\Phi_m(x)}{\mu_{rk}} dx. \tag{5}$$

By enforcing the remaining boundary conditions, i.e., continuity of magnetic fields on the aperture surfaces at $z = t_{i-1}$ and t_i (Fig. 5), we then obtain the integral equations with respect to the aperture fields. Applying Galerkin's procedure to these integral equations, we obtain determinantal equations for the aperture fields. Once the aperture fields are determined, the S-parameters S_{11} and S_{21} can be extracted by calculating the inner products of the eigenmode functions of the guiding waveguide with the aperture fields at the input and output interfaces, respectively.

III. Numerical Procedure and Results

The numerical procedure is based on Galerkin's method. In this procedure, the unknown aperture fields $e_i(x)$ are expanded in terms of the adequate basis functions $f_k^{(i)}(x)$

$$e_i(x) = \sum_{k=1}^{N} a_k^{(i)} f_k^{(i)}(x). \tag{6}$$

The flexible sub-sectional basis functions are utilized to express the aperture fields in this work to adapt wide varieties of objects, lossless or lossy, and moderate or high permeability obstacle materials. The matrix size in this method is the order of the total number of basis functions, and is much smaller than that of the conventional mode-matching method, whose matrix size is the order of the number of eigenfunctions.

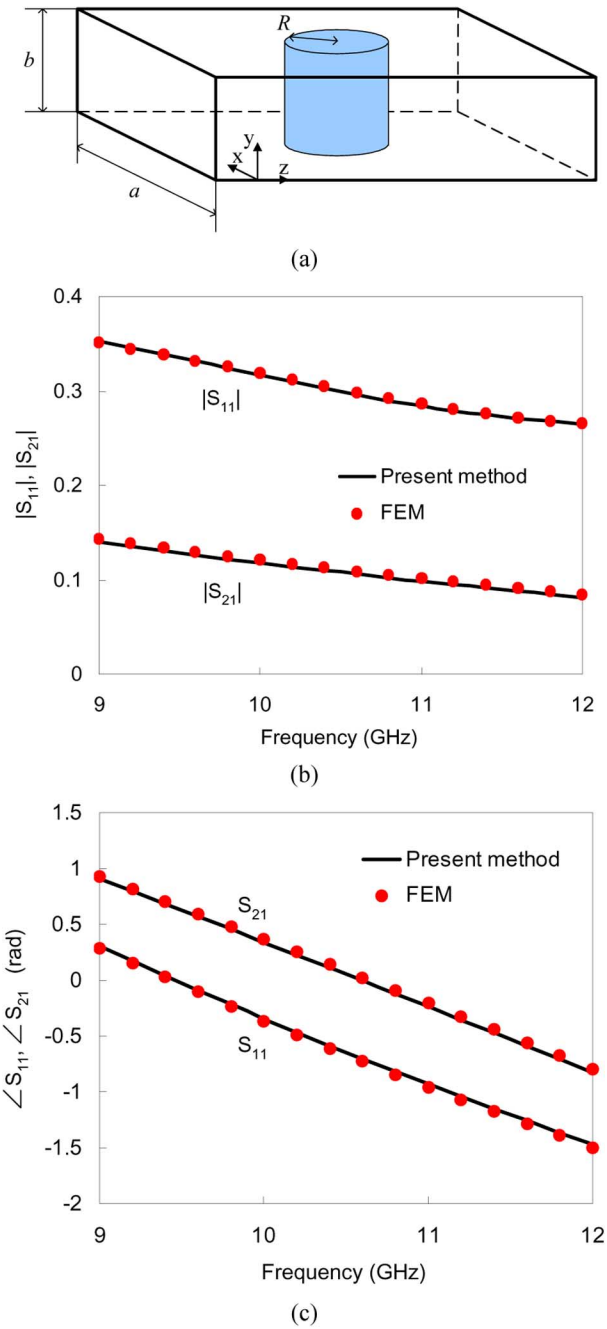

Fig. 6. Frequency-dependent scattering characteristics of a circular post. $\dot{\varepsilon}_r = 5.0 - j1.0$, $\dot{\mu}_r = 2.0 - j0.5$, $R = 7.00$ mm, $a = 22.86$ mm, and $b = 10.16$ mm.

Preliminary computations were carried out to confirm the validity of the proposed method. The frequency-dependent scattering characteristics of a circular post placed in the waveguide [see Fig. 6(a)] are shown in Fig. 6(b) and (c). The S-parameters calculated by the present hybrid EM method and finite-element method (FEM) are in good agreement over the operating frequency range of WR-90, as shown in these figures. Fig. 7 shows the converging characteristics with regard to the number of stair steps for a circular post [see Fig. 6(a)]. It is observed in the figure

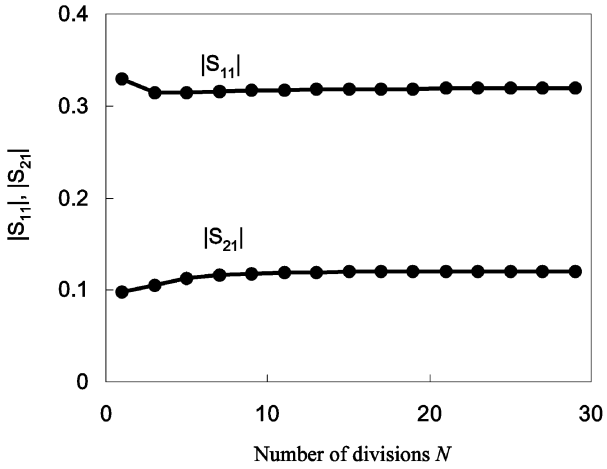

Fig. 7. Converging tendency with number of divisions N at 10 GHz.

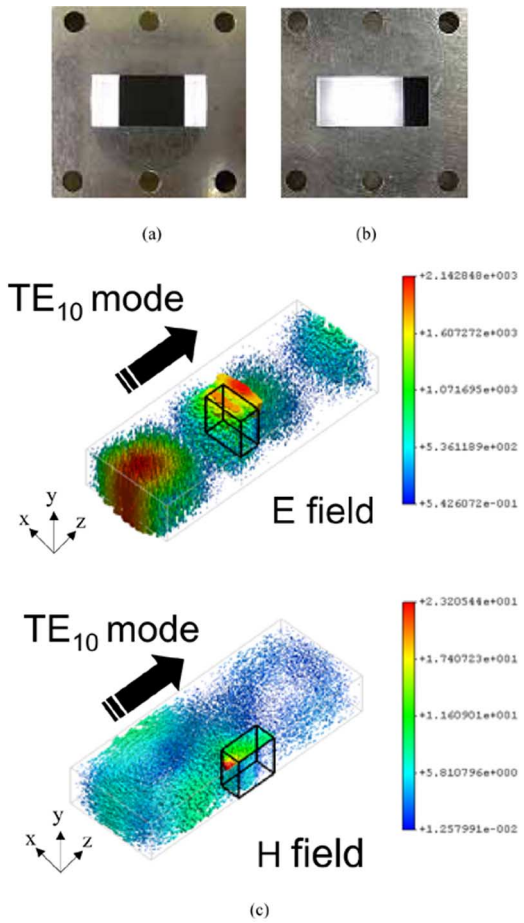

Fig. 8. Location of sample and field distribution of TE_{10} mode.

that the 21 stair steps are sufficient to reach a stable result. Data acquisition with this evaluation method can be processed accurately even by using a personal computer with a Pentium 4 (2 GHz) chip, and the computing time is less than a few seconds. The present hybrid EM method is efficient and suitable for iterative fitting to estimate the material characteristics.

In this study, we measured a sample with both complex permittivity and permeability. When the sample was placed at the center of the test fixture, where the electric field is strong [see Fig. 8(a)], the transmission coefficient is influenced more by the

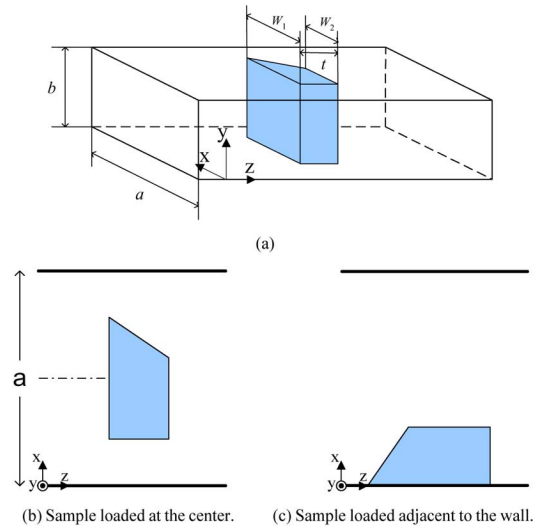

Fig. 9. Columnar sample with trapezoidal cross section in a waveguide. $W_1 = 8.00$ mm, $W_2 = 6.00$ mm, $t = 5.00$ mm, $a = 22.86$ mm, and $b = 10.16$ mm.

TABLE I
REPRODUCTION OF $\dot{\varepsilon}_p$ AND $\dot{\mu}_p$. (TRAPEZOIDAL CROSS SECTION, 10 GHz)

Preassigned		Estimated	
ε' - jε"	μ' - jμ"	ε' - jε"	μ' - jμ"
10.00 - j 2.00	3.00 - j 1.20	10.02 - j 1.99	2.99 - j 1.20
5.00 - j 1.50	2.00 - j 0.50	5.01 - j 1.51	2.00 - j 0.50
2.00 - j 0.50	1.20 - j 0.24	2.00 - j 0.50	1.19 - j 0.23

permittivity of the sample. On the other hand, when the sample is placed adjacent to the wall of the test fixture where the magnetic field is strong [see Fig. 8(b)], the transmission coefficient is influenced more by the permeability of the sample. Therefore, the best suited $\dot{\varepsilon}_r$ and $\dot{\mu}_r$, which provide the minimum deviation ΔS_{21} between the measured and calculated scattering parameters, can be found by performing two processes alternately. That is, in the first process, only $\dot{\varepsilon}_r$ is varied to obtain the minimum deviation ΔS_{21} for the sample placed at the center of the test fixture. Next, $\dot{\varepsilon}_r$ is fixed at the optimal value, and only $\dot{\mu}_r$ is varied to get the minimum ΔS_{21} for the sample placed adjacent to the test fixture wall. The estimation of $\dot{\varepsilon}_r$ and $\dot{\mu}_r$ can be obtained by repeating these almost separate processes alternately.

A virtual experiment was performed to investigate the accuracy of the above estimation process as an inverse problem. A columnar sample with a trapezoidal cross section was placed in the waveguide (Fig. 9). First, the permittivity and permeability of the sample material were set to $\dot{\varepsilon}_p$ and $\dot{\mu}_p$ (preassigned). Complex scattering parameters with the sample loaded at the center [see Fig. 9(b)] and loaded adjacent to the wall of the test fixture [see Fig. 9(c)] are simulated by a commercial FEM simulator using preassigned $\dot{\varepsilon}_r$ and $\dot{\mu}_p$. The complex scattering parameters calculated by the FEM are assumed to be the virtually measured S-parameters, and the permittivity and permeability $\dot{\varepsilon}_r$ and $\dot{\mu}_r$ are assumed to be unknown hereafter. $\dot{\varepsilon}_r$ and $\dot{\mu}_r$ were estimated by the above process using the hybrid EM method. The initial values are selected by trial and error. Table I shows a comparison of the preassigned $\dot{\varepsilon}_p$ and $\dot{\mu}_p$ and the estimated $\dot{\varepsilon}_r$

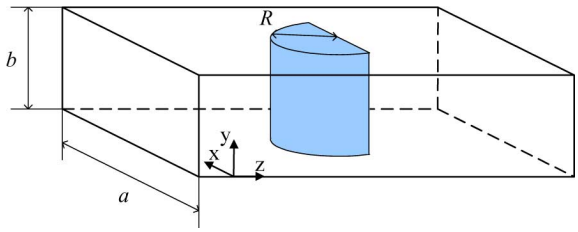

Fig. 10. Columnar sample with semicircular cross section in a waveguide. $R = 3.50$ mm, $a = 22.86$ mm, and $b = 10.16$ mm.

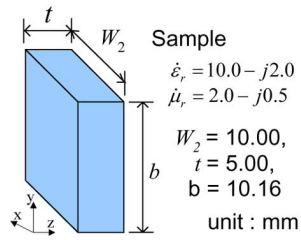

Fig. 11. Columnar sample with a rectangular cross section.

TABLE II
REPRODUCTION OF $\dot{\varepsilon}_p$ AND $\dot{\mu}_p$. (SEMICIRCULAR CROSS SECTION, 10 GHz)

Preassigned		Estimated	
ε' - jε"	μ' - jμ"	ε' - jε"	μ' - jμ"
10.00 - j 2.00	3.00 - j 1.20	10.00 - j 2.00	2.99 - j 1.20
5.00 - j 1.50	2.00 - j 0.50	4.99 - j 1.50	1.99 - j 0.50
2.00 - j 0.50	1.20 - j 0.24	1.99 - j 0.49	1.20 - j 0.24

and $\dot{\mu}_r$, which were obtained after four iterations. An accurate reproduction was observed. The same estimated values $\dot{\varepsilon}_r$ and $\dot{\mu}_r$ are obtained whether the iterative process starts with the case for the sample placed at the center or it starts with the one placed adjacent to the guide wall. A similar virtual experiment was performed for a columnar sample with a semicircular cross section (Fig. 10), and again accurate reproduction can be observed in Table II.

In the present characterization method, the complex permittivity $\dot{\varepsilon}_r$ and permeability $\dot{\mu}_r$ of a sample are evaluated by measuring S_{21} parameters for two different locations of the sample. It is then necessary to determine the errors due to uncertainties in the measurement of the sample positions. The error analysis was performed for the rectangular post shown in Fig. 11. Fig. 12 shows the error rates caused by deviation of the position of the sample loaded at the center of the X-band waveguide [see Fig. 12(a)], while no deviation of the position is assumed for the sample loaded adjacent to the sidewall. The relative error of the real part of the permittivity $\Delta\varepsilon'/\varepsilon'$ at 10 GHz is -0.013% for the 1% deviation of position $\Delta x/W_2$ and is smaller than that of the imaginary part $\Delta\varepsilon''/\varepsilon''$ (-0.053%). The relative errors of the real and imaginary parts of the permeability, $\Delta\mu'/\mu'$ and $\Delta\mu''/\mu''$, are -0.016% and 0.018%, respectively. Fig. 13 shows the error rates caused by deviation of the position of the sample loaded adjacent to the side wall [see Fig. 13(a)], while no deviation of the position is assumed for the sample loaded at the center. The relative errors of of the real and imaginary parts of the permittivity $\Delta\varepsilon'/\varepsilon'$ and $\Delta\varepsilon''/\varepsilon''$ are 0.437% and 0.340% for the 1% deviation of position (air gap) $\Delta x/t$, and those of the permeability $\Delta\mu'/\mu'$ and $\Delta\mu''/\mu''$ are 0.477% and -0.548%, respectively.

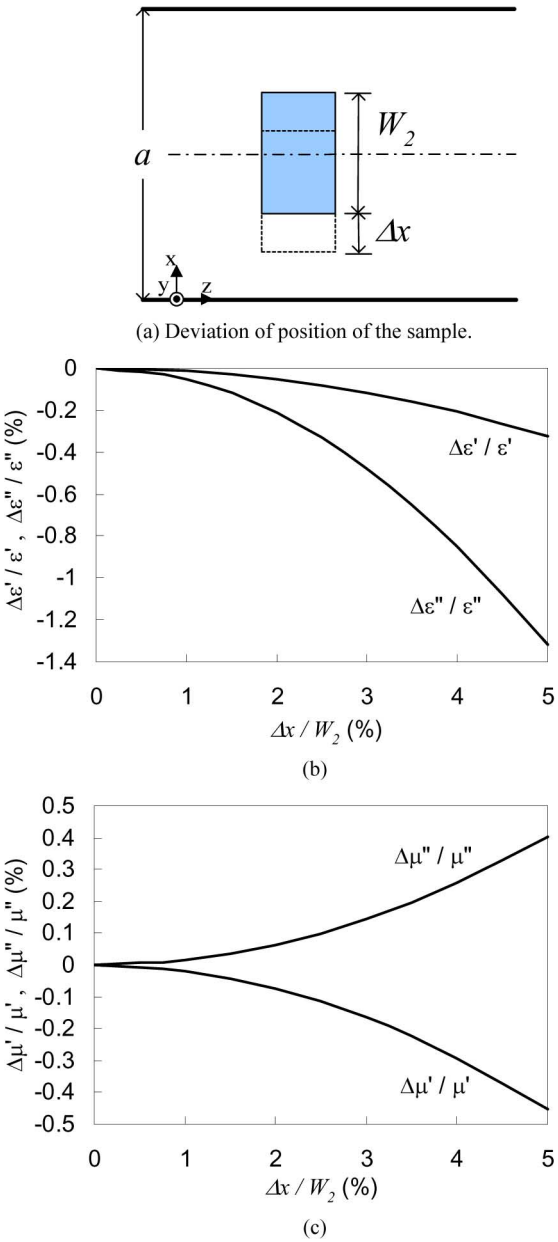

Fig. 12. Error rates of caused by the deviation of position at 10 GHz.

IV. MEASUREMENT SETUP AND RESULTS

A. Measurement Setup

The experimental setup for the evaluation of the material parameters is shown in Fig. 14. X-band waveguides (WR-90; 22.86 mm $\times$ 10.16 mm) are used as guiding lines. The test fixture, made of a 15-mm-long waveguide with the same cross-sectional size as WR-90, is placed between two (input and output) guiding lines. The guiding waveguides are connected to a vector network analyzer (VNA) (Agilent 8719ET) through the waveguide to coax adapters and coaxial cables. The measurement of the reflection parameter S_{11} is not required

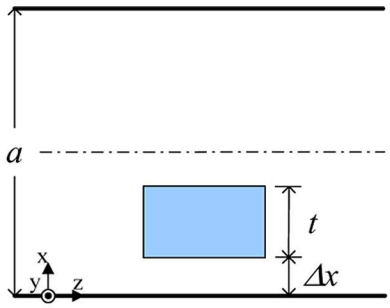

(a) Air gap between the sample and the side wall.

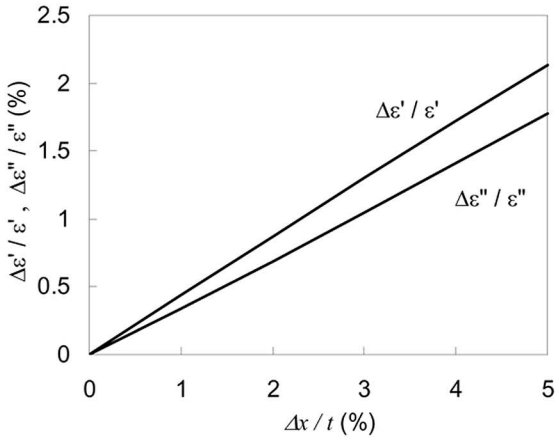

(b)

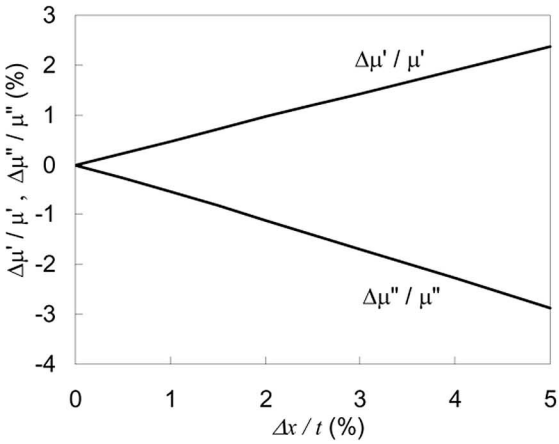

(c)

Fig. 13. Error rates of caused by the air gap at 10 GHz.

in this evaluation method. We only measured S_{21} parameters for two different locations, e.g., with the sample placed at the center and adjacent to the sidewall of the test fixture. We also use the differences between the loaded and unloaded sample data instead of the absolute values of S_{21} to evaluate the material parameters. While measurement of the absolute values of scattering parameters requires the accurate position determination of the sample from the port or reference, the difference of S_{21} between the loaded and unloaded sample is not subject to position error in the axial direction and can be obtained easily and accurately.

Fig. 14. X-band waveguide (WR-90) measurement system.

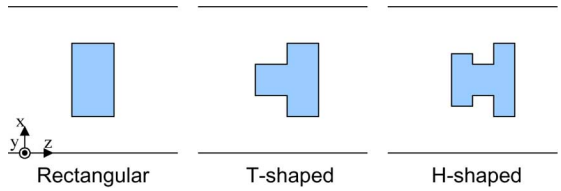

Fig. 15. Allocations of samples.

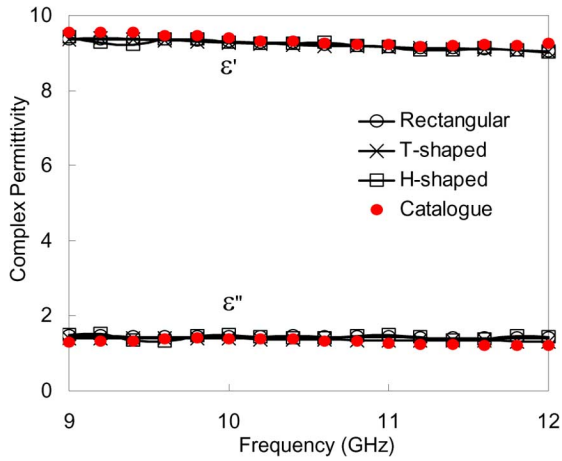

Fig. 16. Frequency dependency of permittivity.

The characteristics of the sample material are estimated by the iterative fitting by numerical calculations, as explained in Section III.

B. Measured Results

Lossy dielectrics, which consists of rubber and carbon powder, is chosen as the sample material. Three different-shaped samples were prepared from the same batch, rectangular-, T-, and H-shaped cross sections. Only complex permittivities are measured for this material and the samples are placed at the center of the test fixture, as shown in Fig. 15. The frequency dependency of complex permittivity $\dot{\varepsilon}_r$ of these samples are shown in Fig. 16, and compared with catalog data (measured with the conventional coaxial line method by the supplier). Good agreement among the measured results is observed over the frequency range. It should be noted that the cutoff frequencies of the dominant TE_{10} mode and the first higher order (TE_{20}) mode of the empty waveguide are 6.56 and

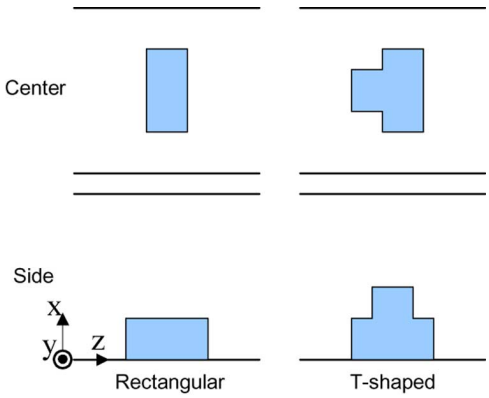

Fig. 17. Allocations of samples.

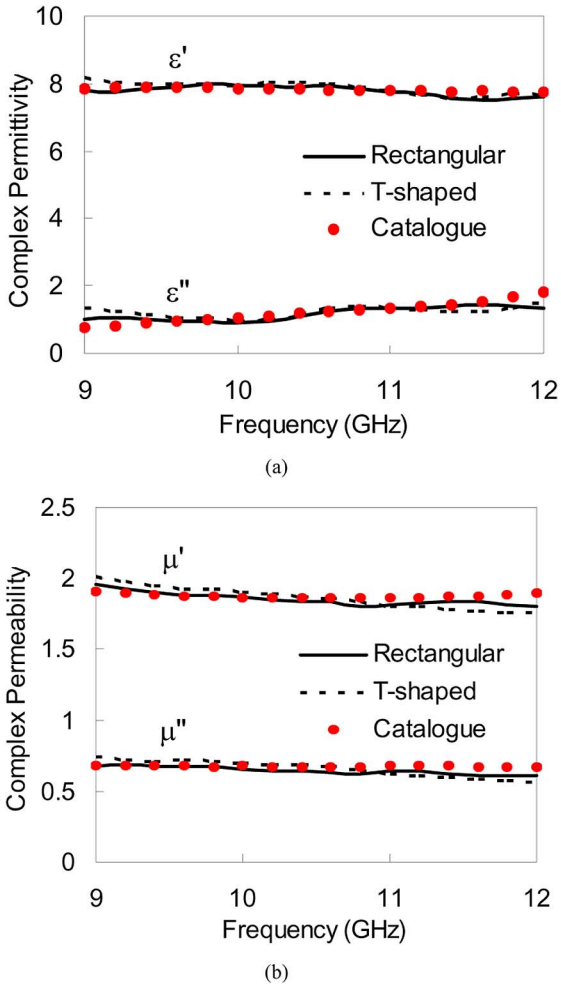

Fig. 18. Frequency dependencies of material constants. (a) Permittivity. (b) Permeability.

13.11 GHz, respectively, and that only the dominant (TE_{10}) mode is propagating in the input and output waveguide over the frequency range, while all the higher order modes become evanescent.

Next, a commercially available microwave absorber (TAKECHI Kogyogomu Co., Ltd.) was used as the sample material with the complex permittivity or permeability. Two different-shaped samples were prepared, i.e., rectangular- and T-shaped cross sections, and they were placed in the test fixture, as shown in Fig. 17. The frequency dependencies of $\dot{\varepsilon}_r$ and $\dot{\mu}_r$ of the two different-shaped samples are shown in Fig. 18, and compared with catalog data (measured with the conventional coaxial line method by the supplier). Good agreement is observed over the measured frequency range, showing the validity of the present procedure. Data acquisition in this measurement method can be processed accurately even using a personal computer with Pentium 4 (2 GHz) and a 1-GB main memory. The computational time is less than 3.1 s for the one frequency point of the sample with rectangular cross sections. The time is less affected by the electrical size of sample, but it increases with the number of layers used in the stairstep approximation of arbitrarily shaped cross section (Fig. 2).

V. Conclusions

We have proposed a practically accurate and effective frequency-dependent evaluation method of materials in the microwave region. This method is based on the accurate and efficient hybrid EM analysis method developed by the authors.

The proposed method requires a single columnar sample, and only measures S_{21} to simultaneously evaluate the complex permittivity $\dot{\varepsilon}_r$ and permeability $\dot{\mu}_r$. The sample needs to have the same height as the holder. however, it may have an arbitrarily shaped cross section and does not require precise processing for measurements. The numerical procedure for the evaluation method uses a smaller sized matrix compared to those in the FEM and the conventional mode-matching method, and the memory requirement for the calculation process is fulfilled by mobile computers. Due to the easy sample preparation, in conjunction with the efficient numerical computations, this method is suitable for characterizing a series of material prototypes on site.

The proposed method can be extended further to evaluate the frequency-dependent characteristics of layered or graded inhomogeneous materials, and these are currently under investigation.

Acknowledgment

The authors would like to thank K. Tahara, Kantoh-Denshi-Ouyou-Kaihatsu, Tokyo, Japan, for his kind supply of test fixtures.

References

[1] J. M. Catalá-Civera, A. J. Canós, F. L. Peñaranda-Foix, and E. R. Davó, "Accurate determination of the complex permittivity of materials with transmission reflection measurements in partially filled rectangular waveguides," *IEEE Trans. Microw. Theory Tech.*, vol. 51, no. 1, pp. 16–24, Jan. 2003.

[2] A. Nishikata, "A swept-frequency measurement of complex permittivity and complex permeability of a columnar specimen inserted in a rectangular waveguide," *IEEE Trans. Microw. Theory Tech.*, vol. 55, no. 7, pp. 1554–1567, Jul. 2007.

[3] S. Yoshikado and I. Taniguchi, "Microwave complex conductivity of a square post in rectangular waveguide," *IEEE Trans. Microw. Theory Tech.*, vol. 37, no. 6, pp. 984–992, Jun. 1989.

[4] C. C. Courtney and W. Motil, "One-port time-domain measurement of the approximate permittivity and permeability of materials," *IEEE Trans. Microw. Theory Tech.*, vol. 47, no. 5, pp. 551–555, May 1999.

[5] A. M. Nicolson and G. F. Ross, "Measurement of the intrinsic properties of materials by time domain techniques," *IEEE Trans. Instrum. Meas.*, vol. IM-19, no. 4, pp. 377–382, Nov. 1970.

[6] W. B. Weir, "Automatic measurement of complex dielectric constant and permeability at microwave frequencies," *Proc. IEEE*, vol. 62, no. 1, pp. 33–36, Jan. 1974.
[7] U. C. Hasar, "A new calibration-independent method for complex permittivity extraction of solid dielectric materials," *IEEE Microw. Wireless Compon. Lett.*, vol. 18, no. 12, pp. 788–790, Dec. 2008.
[8] K. S. Champlin and G. H. Glover, "'Gap effect' in measurement of large permittivities," *IEEE Trans. Microw. Theory Tech.*, vol. MTT-14, no. 8, pp. 397–398, Aug. 1966.
[9] H. Yoshitake, H. Miyagawa, T. Nishikawa, K. Wakino, and T. Kitazawa, "Evaluation of complex permittivity of materials partially filled in coaxial line by using hybrid numerical method," in *Proc. Asia–Pacific Microw. Conf.*, Dec. 2006, pp. 1457–1460.
[10] H. Miyagawa, M. Tsuji, T. Nishikawa, K. Wakino, and T. Kitazawa, "Simultaneous measurement method of complex permittivity and permeability of materials partially filled in rectangular waveguide," (in Japanese) *IEICE Trans. Electron.*, vol. J89-C, no. 12, pp. 1047–1053, Dec. 2006.
[11] H. Miyagawa, K. Hirose, T. Nishikawa, K. Wakino, and T. Kitazawa, "Determination of complex permittivity and permeability of materials in rectangular waveguide using accurate hybrid numerical calculation," in *Eur. Microw. Conf.*, Oct. 2005, vol. 1, pp. 501–504.
[12] H. Miyagawa, T. Nishikawa, K. Wakino, Y.-D. Lin, and T. Kitazawa, "Determination of complex permittivity of columnar materials with arbitrarily-shaped cross section in rectangular waveguide," in *Proc. Asia–Pacific Microw. Conf.*, Dec. 2007, pp. 613–615.
[13] T. Kitazawa, "Nonreciprocity of phase constants, characteristics impedances, and conductor losses in planar transmission lines with layered anisotropic media," *IEEE Trans. Microw. Theory Tech.*, vol. 43, no. 2, pp. 445–451, Feb. 1995.
[14] T. Kitazawa, Y. Hayashi, and M. Suzuki, "Analysis of the dispersion characteristics of slot line with thick metal coating," *IEEE Trans. Microw. Theory Tech.*, vol. MTT-28, no. 4, pp. 387–392, Apr. 1980.
[15] T. Shiraishi, T. Nishikawa, K. Wakino, and T. Kitazawa, "An efficient analysis of lossless and lossy discontinuities in waveguide using hybrid numerical method," *IEICE Trans. Electron.*, vol. E86-C, no. 11, pp. 2184–2190, Nov. 2003.
[16] H. Esteban, S. Cogollos, A. Vidal, V. E. Boria, and M. Ferrando, "A new hybrid mode-matching method for the analysis of inductive obstacles and discontinuities," in *Proc. IEEE AP-S Int. Symp.*, Jul. 1999, vol. 2, pp. 966–969.
[17] R. F. Harrington, *Time–Harmonic Electromagnetic fields*. Piscataway, NJ: IEEE Press, 2001, ch. 3, sec. 3–5, pp. 106–110.

Hayato Miyagawa was born in Matsusaka, Japan, on December 23, 1980. He received the B.E., M.E., and D.E. degrees in electronics engineering from Ritsumeikan University, Shiga, Japan, in 2004, 2006, and 2009, respectively.

His research interests include the material characterization and measurement in microwave/millimeter-wave frequencies.

Kikuo Wakino (M'72–SM'89–F'92–LF'99) received the B.S. degree in physics and Ph.D. degree in electrical engineering from Osaka University, Osaka, Japan, in 1950 and 1980, respectively.

In 1952, he joined the Murata Manufacturing Company Ltd., Kyoto, Japan, as a Research Engineer involved with electronic ceramics for ceramic capacitors, piezoelectric ceramic devices, and microwave dielectric resonator and multichip modules (MCMs). From 1992 to 2003, he was a Visiting Professor with the Institute of Science and Technology, Ritsumeikan University, Kusatsu, Japan. He is currently an Advisor with the Institute of Science and Technology, Ritsumeikan University.

Dr. Wakino is a Fellow of the American Ceramic Society. He is a member of the Japan Ceramic Society.

Yu-De Lin (M'00) received the B.S. degree in electrical engineering from National Taiwan University, Taipei, Taiwan, in 1985, and the M.S. and Ph.D. degrees in electrical engineering from The University of Texas at Austin, in 1987 and 1990, respectively.

In 1990, he joined the faculty of Department of Communication Engineering, National Chiao Tung University, Hsinchu, Taiwan, where he is currently a Professor. His recent research interests include microwave and millimeter-wave printed antennas, propagation characteristics and applications of leaky-wave structures, and design of integrated components for wireless communication.

Toshihide Kitazawa (M'84–SM'89) received the B.E., M.E., and D.E. degrees in electronics engineering from Hokkaido University, Sapporo, Japan, in 1972, 1974, and 1977, respectively.

From 1979 to 1980, he was a Post-Doctoral Fellow with the Japan Society for the Promotion of Science. In April 1980, he joined the Kitami Institute of Technology, Kitami, Japan, as an Associate Professor of electronic engineering. From 1982 to 1984, he was a Visiting Assistant Professor of electrical engineering with the University of Illinois at Urbana-Champaign. From 1989 to 1990, he was a Visiting Scholar of electrical and computer engineering with The University of Texas at Austin. In September 1991, he joined Ibaraki University, Hitachi, Japan, as an Associate Professor of electrical engineering. In April 1996, he joined Ritsumeikan University, Kusatsu, Japan, as a Professor of electrical and electronic engineering. From 2003 to 2005, he was a Visiting Professor with the Shiga University of Medical Science.